ePublishing

ΕΘΝΙΚΟ ΚΕΝΤΡΟ ΤΕΚΜΗΡΙΩΣΗΣ
EKT NATIONAL DOCUMENTATION CENTRE

HNPS Advances in Nuclear Physics

Vol 9 (1998)

HNPS1998

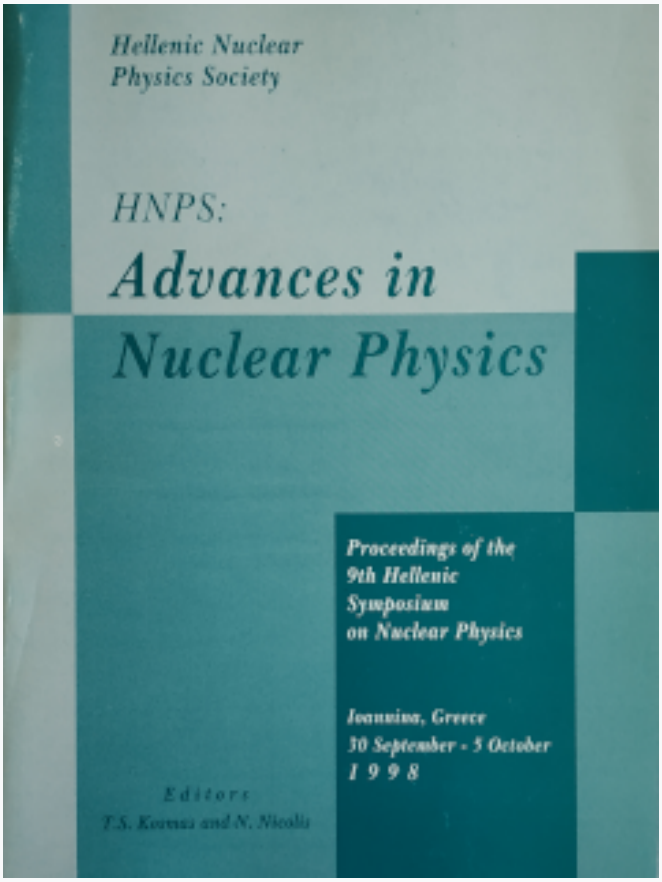

Recent highlights on neutrino-nucleus interactions

E. Kolbe, T. S. Kosmas

doi: 10.12681/hnps.2776

To cite this article:

Kolbe, E., & Kosmas, T. S. (2020). Recent highlights on neutrino-nucleus interactions. *HNPS Advances in Nuclear Physics*, *9*, 63–92. https://doi.org/10.12681/hnps.2776

https://epublishing.ekt.gr | **e-Publisher:** EKT | **Downloaded at:** 12/05/2026 21:11:56

Recent highlights on neutrino-nucleus interactions

E. Kolbe [a] and T.S. Kosmas [b]

[a] *Department für Physik und Astronomie, Universität Basel, Basel, Switzerland*

[b] *Division of Theoretical Physics, University of Ioannina, Greece*

Abstract

The recent developments on neutrino-nucleus interactions at low and intermediate energies are reviewed and discussed in conjunction with the recent data of atmospheric, solar, and accelerator neutrino experiments. The theoretical nuclear physics approaches used to interpret and predict phenomena for which neutrinos play a crucial role are also investigated. We emphasize on the implications of neutrino reactions and properties into the astrophysical phenomena and atmospheric neutrino problems.

1 Introduction

Neutrinos play a fundamental rôle in a plethora of phenomena related to nuclear physics, particle physics, astrophysics and cosmology [1–5]. The main goal of experimental [6–11] and theoretical [12–16] investigations in phenomena involving neutrinos is to discover the yet-unknown properties of these very light and weakly interacting particles and shed light on the relevant open problems to which neutrinos are absolutely crucial. Some of the most significant such phenomena are those involving neutrino–nucleus interactions like the following.

(i) Neutrino–nucleus reactions using well-defined terrestrial sources of low- and intermediate-energy neutrinos. In these accelerator-based experiments the neutrino–nucleus scattering plays an important rôle [17–21], e.g. to detect and distinguish neutrinos of different flavor and to study their interaction with matter.

(ii) Terrestrial experiments to detect astrophysical neutrinos, i.e. solar, supernova, atmospheric, etc., neutrinos [22–28], which are highly valuable sources of astrophysical information.

(iii) Neutrino-induced nucleosynthesis which underlines the neutrino–nucleus interaction within astrophysical scenarios (core-collapse supernovae) and constitutes a good example of interplay of neutrino properties and interactions.

(iv) The investigation of neutrino scattering off nuclei [18] is an ideal tool to examine the basic structure of the weak interactions, since specific transitions between discrete nuclear states with well-defined quantum numbers (spin, parity and isospin) allows us to study the structure of the weak hadronic currents. In such transitions the nucleus acts as a microscopic 'spin–isospin' filter reducing the rather complex spin–isospin structure of weak hadronic currents to a single accurately measurable component.

(v) Neutrino–nucleus reactions are also of great importance to obtain definite information on phenomena like neutrino oscillations and the Mikheyef–Smirnof–Wolfenstein (MSW) effect [28]. In this case the flavor of a neutrino can be identified by the various types of processes. In the Sudbury neutrino observatory (SNO), for example, charged-current (CC) and neutral-current (NC) reactions of neutrinos with deuterons are separately registered with a low detection threshold, thus providing useful information on the neutrino flux for individual flavors and neutrino oscillations as well.

The rich variety of neutrino–nucleus reactions and the great number of promising nuclear targets for the various neutrino experiments combined with the wide range of neutrino energy E_ν necessitated the use of several theoretical nuclear physics approaches. The choice of a specific nuclear method to be employed is dictated among others by the number of available channels in the specific reaction type. Exclusive processes need the use of state-by-state calculations [18]. For inclusive processes accurate effective methods like Fermi gas models [28], closure approximation [13], etc., can also be used because they are more convenient. Semi-inclusive processes, occurring mainly in radiochemical experiments [29,30], need special treatment and various methods have been employed such as continuum RPA [18], local density approximation (LDA) [16], etc. The characteristic ingredients of the nuclear methods, used to obtain reliable estimates of neutrino–nucleus transition matrix elements, are based on a given neutrino–nucleus effective interaction Hamiltonian (see Sect. 2). Among the confidence tests for the employed method, the (p, n)-reaction data constitute important calibrators of the Gamow–Teller-type matrix elements.

In the present work we focus on phenomena mainly related to the standard neutrino–nucleus interaction processes. We only briefly refer to the most important non-standard problems for which the knowledge of neutrino properties is essential. Such a notable example is flavor violation in neutrino-oscillation data [31], of which the current evidence arises from the atmospheric-neutrino anomaly, the solar-neutrino problem and the LSND experimental data [32] although not yet verified by other experiments, KARMEN data, etc.

We firstly review the theory of neutrino–nucleus reactions (Sect. 2). We then present the latest experimental results on exclusive, inclusive and semi-inclusive processes and compare them with reliable theoretical predictions (Sect. 3). The implications of neutrino–nucleus interactions on astrophysical and atmospheric-neutrino problems are discussed with a special emphasis (Sect. 4). Finally, we summarize the main conclusions and discuss the perspectives on the open neutrino problems (Sect. 5).

2 The Theory of Neutrino–Nucleus Interactions

2.1 The Effective Weak Interaction Hamiltonian

The neutrino–nucleus processes can be classified into four categories: the two types of charged-current (CC) reactions of neutrinos and antineutrinos and the two types of neutral-current (NC) ones.

In the *charged-current reactions* a neutrino (antineutrino) of flavor l ($l = e, \mu, \tau$) transforms one neutron (proton) of a nucleus to a proton (neutron), and the corresponding charged (anti)lepton is emitted. These two types of reactions, which are represented by

$$\begin{aligned} \overline{\nu}_l + {}_Z A_N &\longrightarrow {}_{Z-1}A^*_{N+1} + l^+ \,, \\ \nu_l + {}_Z A_N &\longrightarrow {}_{Z+1}A^*_{N-1} + l^- \,, \end{aligned} \tag{1}$$

are also called (anti)neutrino capture, in analogy to the reverse processes of electron, muon or tau capture. They are mediated by exchange of heavy $W^{\pm}$ bosons. A Feynman diagram of lowest order for neutrino capture is shown in Fig. 1.

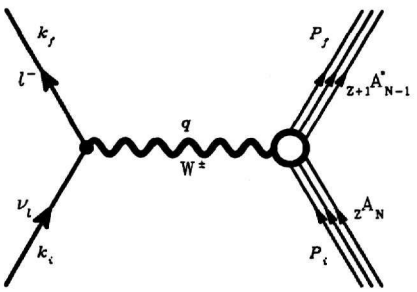

Fig. 1. Feynman-diagram of lowest order for the CC neutrino reactions: $\nu_l + {}_Z A_N \longrightarrow {}_{Z+1}A^*_{N-1} + l^-$

In *neutral-current reactions* (neutrino scattering) the (anti)neutrinos interact *via* exchange of neutral Z^0 bosons with the nucleus, and therefore the charges of projectile and target are both conserved as

$$\begin{aligned} \overline{\nu} + {}_Z A_N &\longrightarrow {}_Z A_N^* + \overline{\nu}' \,, \\ \nu + {}_Z A_N &\longrightarrow {}_Z A_N^* + \nu' \,. \end{aligned} \tag{2}$$

Here we prefer to use ν ($\overline{\nu}$) to denote (anti)neutrinos of any given flavor. The relevant Feynman diagram of lowest order for neutrino scattering is shown in Fig. 2.

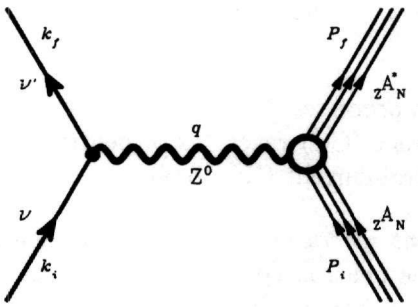

Fig. 2. Feynman-diagram of lowest order for the NC neutrino processes: $\nu + {}_Z A_N \longrightarrow {}_Z A_N^* + \nu'$

The standard-model effective Hamiltonian governing the semileptonic weak interactions of nuclei with neutrinos in (1) and (2) (at low energies compared to the electroweak scale) can effectively be written in current–current form as

$$\mathcal{H}_{\text{eff}} = \frac{G_F}{\sqrt{2}} \left(j_\lambda^{(-)} J^{\lambda(+)} + j_\lambda^{(0)} J^{\lambda(0)} + \text{h. c.} \right) . \tag{3}$$

where $j_\lambda^{(c)}$ and $J^{\lambda(c)}$ denote the leptonic and hadronic currents, respectively, and $c = -, +, 0$ indicates the charge-changing character. According to V–A theory and flavor universality of the weak interaction the leptonic currents are given by

$$\begin{aligned} j_\lambda^{(-)}(x) &= \sum_l \; \overline{\Psi}_l(x) \gamma_\lambda (1 - \gamma_5) \Psi_{\nu_l}(x), \qquad l = e,\ \mu,\ \tau \\ j_\lambda^{(0)}(x) &= \sum_l \; \overline{\Psi}_{\nu_l}(x) \gamma_\lambda (1 - \gamma_5) \Psi_{\nu_l}(x), \qquad l = e,\ \mu,\ \tau \end{aligned} \tag{4}$$

where Ψ_l, Ψ_{ν_l} are the lepton spinors ($j_\lambda^{(+)}$ results from Hermitian conjugation of $j_\lambda^{(-)}$).

More expenditure is required to write down the expressions for the hadronic currents, because nucleons are extended objects. The general ansatz for the hadronic currents is dictated by Lorentz covariance and gives [24,25]

$$J_\lambda^{(c)} = \overline{\Psi}_N \left[g_1^V(q^2)\gamma_\lambda + \frac{i}{2M} g_2^V(q^2)\sigma_{\lambda\nu}q^\nu + g_3^V(q^2)q_\lambda \right.$$
$$\left. + g_1^A(q^2)\gamma_\lambda\gamma_5 + \frac{i}{2M} g_2^A(q^2)\sigma_{\lambda\nu}q^\nu\gamma_5 + g_3^A(q^2)q_\lambda\gamma_5 \right] \tau_c \Psi_N \,, \tag{5}$$

where the weak form factors g_i^V, g_i^A $(i = 1, 2, 3)$ are complex scalar functions of the momentum transfer q^2. The g_i^V are fixed by the conserved vector-current theory (CVC) stating that the isovector part of the electromagnetic current and the charge raising and lowering parts of the vector current of the weak interaction form an isospin triplet of conserved currents. For the axial form factors g_i^A, charge symmetry properties and T-invariance of the hadronic current require that $g_2^A(q^2) = 0$. Furthermore, the $g_3^A(q^2)q_\lambda\gamma_5$ term only gives contributions proportional to the mass of the outgoing lepton, and can therefore be neglected in the extreme relativistic limit. Thus one arrives at the expressions

$$J_\lambda^{(+)} = \overline{\psi}_N \left\{ \left[\frac{F_1^p - F_1^n}{2} \right] \gamma_\lambda \right.$$
$$\left. + \frac{i}{2M} \left[\frac{F_2^p - F_2^n}{2} \right] \sigma_{\lambda\nu}q^\nu + G_A\gamma_\lambda\gamma_5 \right\} \tau_c \Psi_N \,, \tag{6}$$

$$J_\lambda^{(0)} = \overline{\psi}_N \left\{ F_1^Z\gamma_\lambda + F_2^Z \frac{i\sigma_{\lambda\nu}q^\nu}{2M} + G_A\gamma_\lambda\gamma_5 \right\} \psi_N \,, \tag{7}$$

($J_\lambda^{(-)}$ is the Hermitian conjugate of $J_\lambda^{(+)}$). Here $F_{1,2}^p$, $F_{1,2}^n$ denote the charge and electromagnetic form factors of proton and neutron, respectively. The weak form factors entering the neutral hadronic currents are given by ($\tau_0 = +1$ for protons and $\tau_0 = -1$ for neutrons)

$$F_{1,2}^Z = \left(\frac{1}{2} - \sin^2\theta_W \right) \left[\frac{F_{1,2}^p - F_{1,2}^n}{2} \right] \tau_0 - \sin^2\theta_W \left[\frac{F_{1,2}^p + F_{1,2}^n}{2} \right] \,, \tag{8}$$

$$G_A = -\frac{1}{2} G_A^3 \tau_0 \,. \tag{9}$$

In the case of neutral-current neutrino scattering, experiments suggest that [33,34], in addition to the valence quarks in the nucleon, the strange quark sea (pairs of $s\overline{s}$ quarks) also contributes to nucleonic properties like, e.g., the proton-spin (EMC effect). For an extensive discussion on this topic see [35,36]. If present, this $s\overline{s}$ sea in the nucleon could also affect the neutral-current neutrino scattering on nuclei, because the Z^0 bosons mediating these

processes can couple to all quarks inside the protons and neutrons of the nucleus as is illustrated in the diagram of Fig. 3.

To describe quantitatively the connection between the $s\bar{s}$ sea in the nucleon and neutral-current neutrino scattering we construct the neutral weak form factors of proton and neutron from the underlying quark currents. This leads [37] to the form factors

$$F_{1,2}^{Z} = \left(\frac{1}{2} - \sin^2\theta_W\right)\left[\frac{F_{1,2}^{p} - F_{1,2}^{n}}{2}\right]\tau_0 - \sin^2\theta_W\left[\frac{F_{1,2}^{p} + F_{1,2}^{n}}{2}\right] - \frac{1}{2}F_{1,2}^{s}\,, \tag{10}$$

$$G_A = -\frac{1}{2}G_A^3\tau_0 + \frac{1}{2}G_A^s\,, \tag{11}$$

instead of those given in (8) and (9). We see that the additional terms $F_{1,2}^{s}$ and G_A^s arising from the $s\bar{s}$ sea are purely isoscalar and, therefore, they do not contribute to charged-current reactions like ν_e capture or β decay. These strangeness form factors are, in general, not well known, but F_1^s, corresponding to the charge form factor, has to vanish at zero-momentum transfer $F_1^s(q^2 = 0) = 0$, because the nucleon is globally strangeless. In the scattering reactions considered in this work only low-momentum transfers are involved and F_1^s can be neglected.

2.2 The formalism for Neutrino–Nucleus cross section calculations

Due to the smallness of the Fermi coupling constant, neutrino scattering cross sections (as well as β decay and lepton-capture rates) can accurately be calculated within the first-order Born approximation. As the initial and final nuclear states have well-defined spins and parities, a multipole analysis of the weak hadronic current at nuclear level can be performed. This has been at

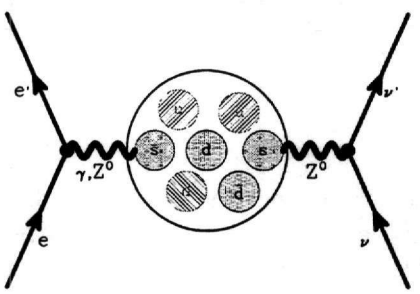

Fig. 3. Leptonic interactions with the proton assuming presence of the strange quark-sea

first carried out [25] in close analogy to electron scattering off nuclei within a general analysis of charge-changing semi-leptonic weak interactions in nuclei.

The neutrino–nucleus scattering differential cross section is then written as

$$\frac{\mathrm{d}^{[2]}\sigma_{i\to f}}{\mathrm{d}\Omega[\mathrm{d}\omega]} = \frac{G^2}{\pi}\frac{|\vec{k}_f|\epsilon_f}{(2J_i+1)}F(Z,\epsilon_f)\left(\sum_{J=0}^{\infty}\eta_{CL}^J + \sum_{J=1}^{\infty}\eta_{TI}^J\right) , \tag{12}$$

where $\omega = \epsilon_i - \epsilon_f$ is the excitation energy of the nucleus, and ϵ_i, ϵ_f, $\vec{k}_f$ denote the energy of the incoming neutrino and energy and momentum of the outgoing lepton, respectively. The square brackets on the left-hand side indicate that the cross section is a double differential, $\mathrm{d}\Omega\mathrm{d}\omega$, i.e. with respect to energy and scattering direction which, strictly speaking, refers rather to excitations lying at the continuum.

The summations in (12) contain the contributions of the charge- ($\widehat{\mathcal{M}}_J$), longitudinal- ($\widehat{\mathcal{L}}_J$) and transverse-operators ($\widehat{\mathcal{T}}_J^{el}$, $\widehat{\mathcal{T}}_J^{mag}$) steaming from the multipole expansion of the weak hadronic current [25]. These contributions are written as

$$\begin{aligned}
\eta_{CL}^J = {} & (1 + a\cos\Phi)\left|\left\langle J_f \left\| \widehat{\mathcal{M}}_J(q) \right\| J_i \right\rangle\right|^2 \\
& + \left(1 + a\cos\Phi - 2b\sin^2\Phi\right)\left|\left\langle J_f \left\| \widehat{\mathcal{L}}_J(q) \right\| J_i \right\rangle\right|^2 \\
& + \left[\frac{\omega}{q}(1 + a\cos\Phi) + c\right] 2\mathrm{Re}\, e \left\langle J_f \left\| \widehat{\mathcal{L}}_J(q) \right\| J_i \right\rangle \left\langle J_f \left\| \widehat{\mathcal{M}}_J(q) \right\| J_i \right\rangle^* , \qquad (13)
\end{aligned}$$

$$\begin{aligned}
\eta_{TI}^J = {} & \left(1 - a\cos\Phi + b\sin^2\Phi\right) \\
& \times \left[\left|\left\langle J_f \left\| \widehat{\mathcal{T}}_J^{mag}(q) \right\| J_i \right\rangle\right|^2 + \left|\left\langle J_f \left\| \widehat{\mathcal{T}}_J^{el}(q) \right\| J_i \right\rangle\right|^2\right] \\
& \mp \left[\frac{(\epsilon_i + \epsilon_f)}{q}(1 - a\cos\Phi) - c\right] \\
& \times 2\mathrm{Re}\, e \left\langle J_f \left\| \widehat{\mathcal{T}}_J^{mag}(q) \right\| J_i \right\rangle \left\langle J_f \left\| \widehat{\mathcal{T}}_J^{el}(q) \right\| J_i \right\rangle^* , \qquad (14)
\end{aligned}$$

where Φ denotes the scattering angle of the outgoing lepton and a, b and c are given by

$$a = \frac{|\vec{k}_f|}{\epsilon_f} = \left[1 - \left(\frac{m_f c^2}{\epsilon_f}\right)^2\right]^{\frac{1}{2}} , \quad b = \frac{\epsilon_i \epsilon_f a^2}{q^2} , \quad c = \frac{(m_f c^2)^2}{q\,\epsilon_f} , \tag{15}$$

where m_f is the mass of the outgoing lepton. The magnitude of the (three-) momentum transfer q is given by

$$q = |\vec{q}| = \left[\omega^2 + 2\epsilon_i\epsilon_f\,(1 - a\cos\Phi) - \left(m_f c^2\right)^2\right]^{\frac{1}{2}} . \tag{16}$$

Notice that the interference term between vector and axial vector current in the lower line of (14) has a negative (positive) sign for (anti)neutrino scattering due to their different helicities.

The Fermi function $F(Z, \epsilon_f)$ takes into account the Coulomb–final-state interaction between nucleus and final lepton (in the case of charged-current reactions only). In other methods like the LDA (see Sect. 3) the final-state interaction effect is considered by modifying the lepton propagator so as to include the lepton self energy (Coulomb potential) which adds to the kinetic energy in the propagator.

2.3 Neutrino Flux-Averaged Cross Section in Various Reaction Processes

In order to compare the theoretical results with the experimental data, the differential cross section of (12) is at first integrated over the scattering angle

$$\frac{[\mathrm{d}]\sigma}{[\mathrm{d}\omega]}(\epsilon_i, [\omega]) = \int_0^{4\pi} \frac{\mathrm{d}^{[2]}\sigma}{\mathrm{d}\Omega[\mathrm{d}\omega]}(\Phi, \epsilon_i, [\omega])\;\mathrm{d}\Omega\,, \tag{17}$$

and then folded with the normalized energy distribution $n_i(\epsilon_i)$ of the incoming neutrinos as

$$\frac{[\mathrm{d}]\overline{\sigma}}{[\mathrm{d}\omega]}([\omega]) = \int_{\omega}^{\infty} \frac{[\mathrm{d}]\sigma}{[\mathrm{d}\omega]}(\epsilon_i, [\omega])\; n_i(\epsilon_i)\;\mathrm{d}\epsilon_i\,. \tag{18}$$

In the case when the neutrino-induced excitation of a specific final state f is measured in an experiment, i.e. for exclusive neutrino–nucleus processes, the relevant cross section $\overline{\sigma}_{i\to f}$ is given by (18).

If the final nuclear state cannot be determined, i.e. for *inclusive neutrino–nucleus reactions*, one must integrate (18) over the possible final states to obtain the total inclusive cross section as

$$\overline{\sigma}_{tot} = \int_0^{\infty} \frac{\mathrm{d}\overline{\sigma}}{\mathrm{d}\omega}(\omega)\;\mathrm{d}\omega\,. \tag{19}$$

Of special importance in the investigation of neutrino–nucleus processes are the semi-inclusive (anti)neutrino–nucleus cross sections which include the part

of the total cross section leading to the particle-bound excited states of the final nucleus; the flux-averaged semi-inclusive cross section is obtained as in (19). In Sect. 3, the comparison between the theoretical and experimental results (for the total, radiochemical experiments and exclusive cross sections) is done in the above spirit.

2.4 Nuclear Calculations for the Neutrino-Nucleus Cross Sections

The first calculations to describe neutrino-induced excitations were done by Überall and Kelly [22,23] for the giant-dipole resonance in ^{12}C within the Goldhaber–Teller model and the shell model [22,23]. At that time physicists contemplated the construction of high-intensity accelerators or 'pion factories', which *via* pion decays would also provide fluxes of electron and muon neutrinos. The motivation to investigate cross sections and angular distributions for neutrino scattering was to get new insights into questions of weak interactions, like proving the possible identity of muon and electron neutrinos [22] and, furthermore, to check the energy spectrum of the produced neutrinos by measuring the rate of theoretically known cross sections [23].

Later on Donnelly and Walecka performed fundamental and comprehensive theoretical studies of semileptonic weak interactions in nuclei [24,25]. Within the shell model they calculated cross sections for neutrino scattering on ^{12}C [26] and ^{16}O [27,26], compared electron-scattering and neutrino-scattering processes [27] and used neutrino excitations of nuclear levels to test the structure of the weak neutral currents [27]. These works were motivated by the expectation that these reactions would be studied experimentally at LAMPF.

Within the last decades many nuclear methods have been developed and used for neutrino–nucleus reaction calculations. Donnelly, Kubodera and others [24,27,28] developed an elementary-particle model applied to describe neutrino scattering on ^{12}C and ^{13}C [38]. The great number of nuclear methods used up to the present for neutrino–nucleus interaction studies are classified as follows.

(i) *Term-by-term sum* [12]. These methods need the explicit construction of the final states in the context of a nuclear model, e.g. shell model, RPA etc. They are reliably applicable for low neutrino energies and for light or medium-heavy nuclei when the transitions to definite nuclear states (ground state or some low-lying excitations) could be dominant.

(ii) *Closure approximation* [13]. With this category of methods one avoids the tedious construction of the excited nuclear states if a suitable mean excitation energy $\overline{E}$ could be chosen. The results of this method depend on the assumed value of $\overline{E}$ and are more reliable for neutrino energies 50 MeV

$\leq E_\nu \leq 100$ MeV.

(iii) *Fermi gas models* [14]. The Fermi gas models, the non-relativistic one and the relativistic one, need an average binding energy which defines the effective energy transfer to the nuclear target. The results are very sensitive to the average binding energy used (in particular at low neutrino energies) and more reliable estimates for neutrino cross sections can be obtained for $E_\nu \geq 50$ MeV where the details of the specific nuclear states can be ignored.

In the present work the latest experimental data on neutrino–nucleus reactions are mainly compared with the theoretical predictions of two nuclear methods, the continuum RPA (CRPA) and the local density approximation which uses a relativistic Lindhard function (LDA). Both these methods give very reliable results especially for the important processes of semi-inclusive and inclusive neutrino–nucleus cross sections. In order to briefly outline the basic features and ingredients of these methods, we devote for each of them an individual subsection.

Continuum Random Phase Approximation

For the description of neutrino scattering off nuclei the continuum RPA approach was employed as a mean-field model [17,18], in order to compute matrix elements of $J^{\lambda(a)}$ when sandwiched between nuclear states. In this model the interaction between the constituents of the nucleus is described by combining the usual RPA treatment with a correct description of the particle states in the continuum, i.e. the excited many-body states are coherent superpositions of one-particle–one-hole ($1p$–$1h$) excitations obeying the proper Coulomb boundary conditions for scattering states. The continuum RPA provides a good description of the nuclear ground state while the excited states are generic continuum states possessing a $1p$–$1h$ structure. Final-state interactions are accounted for by a realistic (finite-range) residual interaction derived from the Bonn meson exchange potential [19,20].

The continuum random phase approximation (CRPA) model is reliable to calculate mainly total cross sections for inclusive and semi-inclusive processes of semileptonic weak interactions in nuclei. The motivation for this choice is explained by means of Fig. 4 where a schematic plot of a cross section for neutrino scattering on nuclei is shown. We assume that the incoming neutrino has a medium energy of $E_\nu \approx 50$ MeV and plot the cross section as a function of the excitation energy ω in an isoscalar target nucleus ($T_i = 0$). As neutrinos dominantly induce isovector transitions ($\Delta T = 1$), it is found that the lowest-lying states that get remarkable strength are (if present at all) a few discrete states with isospin $T_f = 1$. Next, above the particle emission threshold ($\omega_{\rm th}$),

small isovector resonances show up and collect some strength. However, the dominant contributions to the total cross section come from the broad states in the giant-dipole resonance (GDR) region, which are known to have the structure of collective one-particle–one-hole (1p–1h) excitations. Lastly, very energetic neutrinos may scatter quasi-elastically (QE) and knock out (single) nucleons from the nucleus. These final nuclear states dominantly excited in neutrino scattering are nicely described by the continuum RPA model.

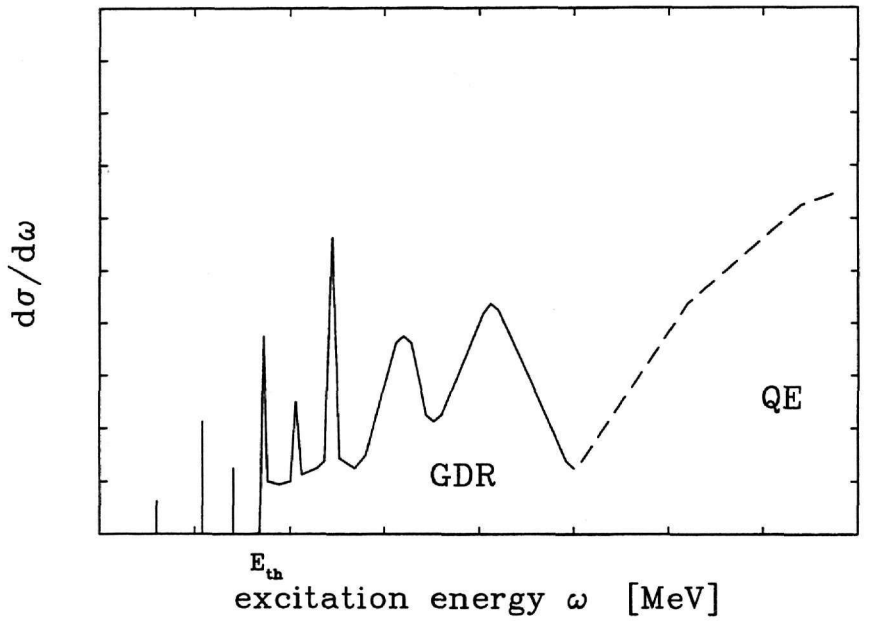

Fig. 4. Schematic plot of a typical cross section for medium energy neutrino scattering on an isoscalar nucleus

The basic properties of this approach can be summarized as follows: (i) the nuclear ground state is well described, (ii) the excited states are generic continuum states of $1p$–$1h$ structure, (iii) final state interactions are accounted for with a realistic (finite-range) residual interaction [19,20], (iv) this model has been shown [18,39] to yield a good description of the giant (dipole and spin-dipole) resonances in light nuclei, e.g. in ^{12}C and ^{16}O, (v) especially the charge-exchange reactions of the knocked-out nucleon of the type $X(\nu, \nu' x)Y$ and $X(\nu_l, l^- x)Y$ are included in the model.

To show how the method works we choose as an example the case of neutrino-induced knock out reactions of the type $X(\nu, \nu' x)Y$ and $X(\nu_l, l^- x)Y$. In the general case, for the neutrino-induced knock out of a particle we need to apply a special treatment to calculate cross sections. A reasonable assumption is to assume that the process takes place in two steps. For example, in the neutral-

current scattering

$$\nu + {}_{Z}X_{N} \rightarrow \nu' + {}_{Z}X_{N}^{*} \Longrightarrow {}_{Z}X_{N}^{*} \rightarrow \begin{cases} {}_{Z-1}X_{N} & + p \\ {}_{Z}X_{N-1} & + n \\ {}_{Z-2}X_{N-2} & + \alpha. \end{cases}$$

In the first step the cross section for neutrino excitation is determined within an effective model calculation and in the second step a state-by-state calculation is more realistic.

In the context of the continuum RPA model the cross section for the first step of the process is calculated by integrating over all the neutrino excitations. In the second step one calculates for each final state with well-defined energy, angular momentum and parity the individual branching ratios into the various decay channels (proton, neutron, α or γ emission) using the statistical model. The code appropriate for this aim, known as SMOKER [40], considers as possible final states in the residual nucleus the experimentally known levels supplemented at higher energies by an appropriate level-density formula [40]. This model has been successfully applied to many astrophysical problems and it empirically found good agreement between p/n branching ratios calculated with SMOKER and within continuum RPA for several neutral-current reactions on light nuclei [41].

The Local-Density Approximation
with a Relativistic Lindhard Function

In this method [15], the differential neutrino–nucleus cross section is expressed as a function of the local Fermi momentum $p_{\mathrm{F}}(r)$ (local-density approximation). In this way both bound as well as excited states (including also the continuum) of the proton and neutron can be taken into account by using the particle–hole excitations involved in a relativistic Lindhard function [15]. In addition, the important effects of Coulomb distortion and renormalization of the operators involved in the elementary neutrino–nucleon process inside the nucleus can be also considered [46,47]. This method was recently improved [16] so that it can give the cross sections for particle-bound nuclear states with which the flux-averaged cross section for radiochemical experiments (semi-inclusive processes) can be calculated.

By assuming a local-density approximation the total neutrino–nucleus reaction cross section σ for the effective Hamiltonian (3) is written as [15]

$$\sigma = -\frac{2G^2 cos^2\theta_c}{\pi} \int_0^R r^2 dr \int_{p_l^{min}}^{p_l^{max}} p_l^2 dp_l \int_{-1}^{1} d(cos\theta) \frac{1}{E_\nu E_l} \overline{\sum}\sum \mid T \mid^2$$
$$\times Im\overline{U}(E_\nu - E_l - Q + Q' - V_C(r), \vec{q})\, \Theta(E_l + V_C(r) - m_l) \qquad (20)$$

where $\overline{\sum}\sum \mid T \mid^2$ stands for the sum and average over final and initial spins of the leptons and nucleons of the T-matrix squared (see appendix of [15]). The function $\Theta(x)$ is the *theta* function, V_C is the Coulomb energy of the lepton and Q is the Q-value of the reaction. The function $Im\overline{U}(q^0, \vec{q})$ represents the imaginary part of the modified Lindhard function [48]. The minimum, $p_l^{min} = 0$, and maximum, $p_l^{max} = [(E_l^{max})^2 - m_l^2]^{1/2}$, lepton momentum are determined by the kinematics, i.e.

$$E_l^{max} = E_\nu - V_C(r) - Q\,. \qquad (21)$$

The quantity Q' in (20) is the difference of the proton and neutron local Fermi energies

$$Q' = E_{p_F} - E_{n_F}\,. \qquad (22)$$

The magnitudes of the momenta p_{F_n} and p_{F_p} are given in terms of the neutron and proton nuclear densities, *via* a local-density approximation and q^2 is written as

$$q^2 \;=\; q_0^2 - \vec{q}^2 \;=\; (E_l - E_\nu)^2 - (\vec{p}_l - \vec{p}_\nu)^2\,, \qquad (23)$$

where $\vec{p}_i$ denotes the three-momentum of the particles involved in the process.

The ordinary Lindhard function [47] takes into account the p, n excitations and it is given by

$$\overline{U}(q^0, \vec{q}) = 2 \int \frac{d^3p}{(2\pi)^3} \left\{ \frac{n(\vec{p})[1 - n(\vec{p}+\vec{q})]}{q^0 + \varepsilon(\vec{p}) - \varepsilon(\vec{p}+\vec{q}) + i\epsilon} \right.$$
$$\left. + \frac{n(\vec{p})[1 - n(\vec{p}-\vec{q})]}{-q^0 + \varepsilon(\vec{p}) - \varepsilon(\vec{p}-\vec{q}) + i\epsilon} \right\}\,, \qquad (24)$$

where $n(\vec{p})$ is the occupation number of the Fermi sea and $\varepsilon(\vec{p})$ the nucleon kinetic energy. When studying the neutrino cross sections at low energies the use of the modified Lindhard function $\overline{U}(q^0, \vec{q})$ [16] becomes necessary because the ordinary one has a pathological behavior at $q^0 = 0$ and $\vec{q} \to 0$.

The difference between a Fermi sea and the finite nucleus is that the denominator of (24) vanishes when $q^0 = 0$ and $\vec{q} \to 0$, which leads to an expression

of the type 0/0 with a finite limit, while in finite nuclei it is zero because the numerator of (24) vanishes when $\vec{q} \to 0$. This is because in nuclear matter one has a continuum of states while in finite nuclei there is a minimum energy needed to excite the first excited state. This energy gap (Δ), which in the case of nuclear systems varies from $\approx$ 6 MeV, for light nuclei, to $\approx$ 1 MeV, for heavy nuclei, is what makes the denominator of the response function different from zero for finite nuclei. In the present LDA calculations the value $\Delta = 3.0$ MeV was used throughout the periodic table.

In general, the LDA method is more reliable for semi-inclusive and total cross section calculations for which it gives very accurate results [15,16].

3 The Latest Experimental Data and its Comparison with Theoretical Predictions

3.1 Accelerator Neutrino Sources

The electron neutrino beams used in experiments (e.g. at LAMPF, KARMEN etc.) are produced from the decay of muons resulting from the decay of slow pions and therefore they have relatively low energies. While the two-body pion decay at rest

$$\pi^+ \to \mu^+ + \nu_\mu \,, \tag{25}$$

produces mono-energetic muon neutrinos with an energy $\epsilon_{\nu_\mu} = 29.8$ MeV, the subsequent μ^+ decay

$$\mu^+ \to e^+ + \overline{\nu}_\mu + \nu_e \,, \tag{26}$$

yields equal fluxes of electron neutrinos and muon antineutrinos. The corresponding spectra from this purely leptonic decay are shown in Fig. 5. They have the characteristic Michel shape [49] with a maximum energy of 52.8 MeV.

At LAMPF (now referred to as the Los Alamos neutron science center, LANSCE) a few percent of the produced π^+ and π^- decay in flight and give rise to the ν_μ and $\overline{\nu}_\mu$ spectrum shown in the lower part of Fig. 5 with neutrino energies up to 300 MeV [50]. Therefore, using these energetic neutrino beams, the LSND Collaboration could also measure the $^{12}\mathrm{C}(\nu_\mu, \mu^-)X$ cross section which has a threshold of 123 MeV.

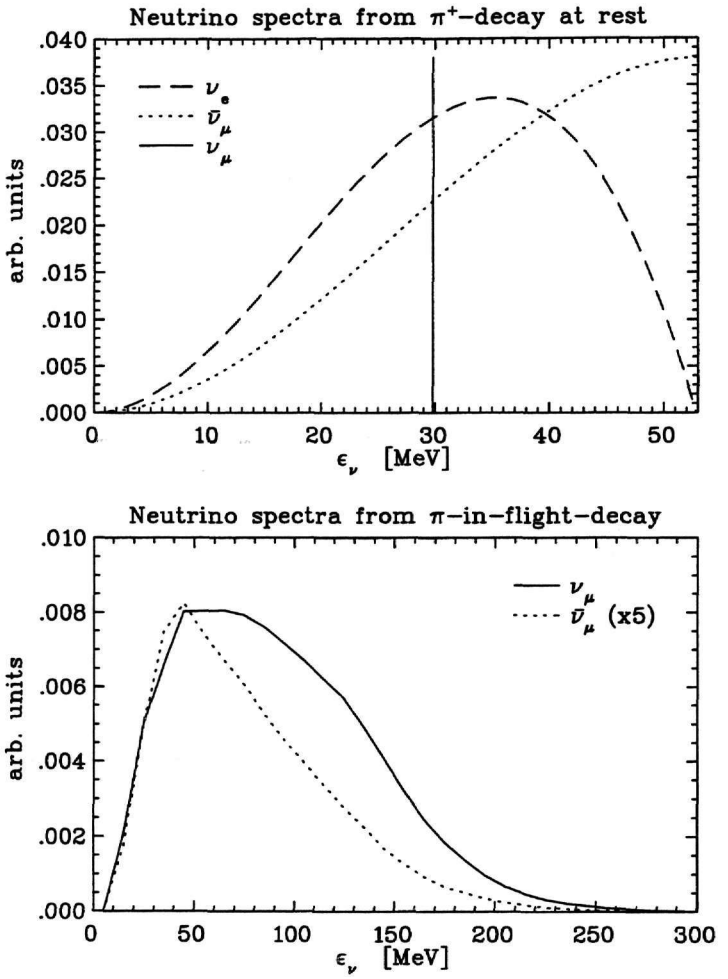

Fig. 5. The 'KARMEN' and 'LSND' neutrino spectra

3.2 Neutrino-Induced Reactions Measured at Accelerators

Recently measurements of cross sections (with an error $\leq$20%) for neutrino–nucleus scattering at accelerators have became feasible. First an experimental group (E225) at LAMPF [51] determined both the inclusive $^{12}C(\nu_e, e^-)X$ cross section and the exclusive contribution to the ^{12}N ground state. The KARMEN Collaboration [7] measured these neutrino-capture processes, too, and for the first time observed a neutral-current excitation of a nucleus, the ^{12}C$(\nu, \nu')^{12}$C$^*(1^+, 1; 15.11$ MeV) reaction. At the beginning of the 1990s the liquid scintillator neutrino detector (LSND) at LAMPF [52] was put into operation and began (within a medium-energy physics program) to study neutrino-induced reactions on ^{12}C.

The main physics aim of the KARMEN and LSND experiments was to search for the appearance of neutrino oscillations in the $\nu_\mu \rightarrow \nu_e$ and $\overline{\nu}_\mu \rightarrow \overline{\nu}_e$ channels. However, the extraction of the neutrino–nucleus interaction cross sections is of substantial importance for the following reasons:

- These measurements provide valuable information about the response of the detector.
- Nuclear reactions serve as detectors for neutrino oscillations (e.g., $^{12}\mathrm{C}(\nu_e, e^-)^{12}\mathrm{N}_{\mathrm{g.s.}}$) and the corresponding cross sections are needed to extract the oscillation parameters from the data.
- They serve for testing the nuclear-structure models.
- The agreement between the calculated and experimental results for the cross section of the channel $^{12}\mathrm{C}(\nu, \nu')^{12}\mathrm{C}^*$ $(1^+, 1; 15.11$ MeV) cross section confirmed the structure of the weak neutral current as given within the standard model [8].
- The measured ratio of the neutral to charged-current-induced cross sections on $^{12}\mathrm{C}$ corresponded to the value expected from theory [10,11], which implied a new test of the ν_e, $\overline{\nu}_\mu$ universality [9].
- An analysis of the electron spectrum from the $^{12}\mathrm{C}(\nu_e, e^-)^{12}\mathrm{N}_{\mathrm{g.s.}}$ reaction has put stringent upper limits on non-standard contributions to the weak charged current [10,11].

Below we compare the recent exclusive and inclusive experimental data with the theoretical predictions of the methods CRPA and LDA.

Exclusive Cross Sections

In Table 1 we quote the results for the exclusive cross sections measured on $^{12}\mathrm{C}$ in the following two cases:

(i) the charged-current electron neutrino, $^{12}\mathrm{C}(\nu_e, e^-)^{12}\mathrm{N}_{\mathrm{g.s.}}$ and the muon neutrino, $^{12}\mathrm{C}(\nu_\mu, \mu^-)^{12}\mathrm{N}_{\mathrm{g.s.}}$, scattering which lead to the ground state of the N nucleus ($^{12}\mathrm{N}_{\mathrm{g.s.}}$).

(ii) the neutral-current neutrino scattering $^{12}\mathrm{C}(\nu, \nu')^{12}\mathrm{C}^*(15.11)$ leading to the excited state $E_x = 15.11$ MeV of the C nucleus [$^{12}\mathrm{C}^*(15.11)$].

In both cases the agreement of the results obtained with the improved CRPA calculation (for two types of residual interactions denoted as $\sigma_{\mathrm{BP}}^{\mathrm{new}}$ and $\sigma_{\mathrm{LM}}^{\mathrm{new}}$) is very good. We also compare the CRPA results with the previous RPA calculation ($\sigma_{\mathrm{BP}}^{\mathrm{old}}$, $\sigma_{\mathrm{LM}}^{\mathrm{old}}$) obtained without partial occupation of the $p_{1/2}$ subshell. As can be seen our agreement with the data is much better, which supports the argument that the subshell $p_{1/2}$ appears to be partially occupied, although $^{12}\mathrm{C}$ is considered as a double closed (sub)shell nucleus.

Table 1
The exclusive cross sections for charged- and neutral-current neutrino scattering (in units of 10^{-42} cm^2). The results of our improved RPA calculation for both of the applied residual interactions ($\sigma^{\rm new}_{\rm BP}$, $\sigma^{\rm new}_{\rm LM}$) are compared to the data and the previous RPA calculation ($\sigma^{\rm old}_{\rm BP}$, $\sigma^{\rm old}_{\rm LM}$) without partial $p_{1/2}$ subshell occupation.

Process	Data	Ref.	$\sigma^{\rm new}_{\rm BP}$	$\sigma^{\rm new}_{\rm LM}$	$\sigma^{\rm old}_{\rm BP}$	$\sigma^{\rm old}_{\rm LM}$
$^{12}C(\nu_e, e^-)^{12}N_{g.s.}$	$10.5 \pm 1.0 \pm 1.0$	[51]				
	$8.9 \pm 0.6 \pm 0.75$	[7]	8.9	8.9	9.3	9.3
	$9.1 \pm 0.4 \pm 0.9$	[32]				
$^{12}C(\nu_\mu, \mu^-)^{12}N_{g.s.}$	$66 \pm 10 \pm 10$	[32]	68	73	63	63
$^{12}C(\nu, \nu')^{12}C^*(15.11)$	$10.4 \pm 1.0 \pm 0.9$	[8]	10.5	10.5	10.5	10.6
$^{12}C(\nu_\mu, \nu'_\mu)^{12}C^*(15.11)$	$3.2 \pm 0.5 \pm 0.4$	[53]	2.8	2.7	2.8	2.8

Inclusive and Semi-inclusive Cross Sections

The inclusive and semi-inclusive cross section data measured by using a ^{12}C target in the accelerator experiments are listed in Table 2. In the case of semi-inclusive processes the charged-current reaction data for both the electron neutrino, $^{12}C(\nu_e, e^-)^{12}N^*$ and the muon neutrino, $^{12}C(\nu_\mu, \mu^-)^{12}N$, leading to $^{12}N^*$ are quoted. We also show the inclusive results of the reaction $^{12}C(\mu^-, \nu_\mu)^{12}B^*$, i.e. the processes which lead to the excited channels of the B nucleus ($^{12}B^*$).

From the comparison with the theoretical results we see that the improved continuum RPA calculations, $(\omega/\sigma)^{\rm new}$, are in good agreement with the data. We also compare the improved CRPA results with the previous, $(\omega/\sigma)^{\rm old}$, continuum RPA calculation without partial $p_{1/2}$ subshell occupation. The latter comparison also suggests the interesting result for the nuclear structure of ^{12}C, that the subshell $p_{1/2}$ is partially occupied.

The results of the flux-averaged cross section $\overline{\sigma}$ obtained with the LDA method are shown in Table 3. In this table we quote in addition the results obtained for the radiochemical cross sections. They have been obtained by setting the integrand of (20) to zero, i.e. by putting $E_\nu - E_e > Q + E^N_{\rm thres} + V_{\rm C}$, where $E^N_{\rm thres}$ represents the smallest of the values $E^p_{\rm thres}$, $E^n_{\rm thres}$, for proton or neutron emission. In this way, the contribution of the excited states above the threshold energies for proton or neutron emission $E^N_{\rm thres}$ is excluded.

We can compare the results of the LDA with those of the recent radiochemical experiment at LAMPF [30] for ^{127}I. The values quoted in [30] give a cross section of $\overline{\sigma} = (6.2 \pm 2.5) \times 10^{-40}$ cm^2. The LDA gives the value $\overline{\sigma} = 4.2 \times 10^{-40}$ cm^2 for this cross section. It is also interesting to compare these results

with two other recent theoretical results. On the one hand, in [43] the values $\overline{\sigma} = 6.4 \times 10^{-40}\,\mathrm{cm}^2$ and $\overline{\sigma} = 3.0 \times 10^{-40}\,\mathrm{cm}^2$ are quoted using two different approaches, which both rely on the closure approximation. We should recall, however, that these are total cross sections and not radiochemical. They should be compared to the result $\overline{\sigma} = 7.3 \times 10^{-40}\,\mathrm{cm}^2$ of the LDA.

On the other hand, in [57] the radiochemical cross section is evaluated by summing over the discrete excited states of ^{127}Xe and a cross section of $\overline{\sigma} = 2.1 \times 10^{-40}\,\mathrm{cm}^2$ is obtained, if $g_A = -1.0$ is used, or $\overline{\sigma} = 3.1 \times 10^{-40}\,\mathrm{cm}^2$, if $g_A = -1.26$ is used. We mention that the LDA method provides an automatic

Table 2
The inclusive muon capture rate ω for ^{12}C (in units of 10^3 s^{-1}) and the cross section σ for the $^{12}\mathrm{C}(\nu_e, e^-)$ $^{12}\mathrm{N}^*$ reaction (in units of 10^{-42} cm^2) and the total (inclusive + exclusive) cross section for the $^{12}\mathrm{C}(\nu_\mu, \mu^-)^{12}\mathrm{N}$ reaction (in 10^{-40} cm^2). The results of our improved continuum RPA calculation ($(\omega/\sigma)^{\mathrm{new}}$) are compared to the data and the previous ($(\omega/\sigma)^{\mathrm{old}}$) continuum RPA calculation without partial $p_{1/2}$ subshell occupation.

Process	Data	Ref.	$(\omega/\sigma)^{\mathrm{new}}_{\mathrm{BP}}$	$(\omega/\sigma)^{\mathrm{new}}_{\mathrm{LM}}$	$(\omega/\sigma)^{\mathrm{old}}_{\mathrm{BP}}$	$(\omega/\sigma)^{\mathrm{old}}_{\mathrm{LM}}$
$^{12}\mathrm{C}(\mu^-, \nu_\mu)^{12}\mathrm{B}^*$	32.8 ± 0.8	[54]	32.7	31.3	34.2	33.3
$^{12}\mathrm{C}(\nu_e, e^-)^{12}\mathrm{N}^*$	$5.1 \pm 0.6 \pm 0.5$	[55]	5.4	5.6	6.3	5.9
	$5.7 \pm 0.6 \pm 0.6$	[56]				
$^{12}\mathrm{C}(\nu_\mu, \mu^-)^{12}\mathrm{N}$	$12.4 \pm 0.3 \pm 1.8$	[56]	17.8	17.5	19.3	20.3

Table 3
Flux-averaged cross section $\overline{\sigma}$ for ν_e obtained by folding the cross section σ in a Michel neutrino-energy distribution (see text). $\overline{\sigma}_{rad}$ contains the contribution of particle bound states only and $\overline{\sigma}_{tot}$ contains the contribution of all accessible particle states of the final nucleus

Reaction	$\overline{\sigma}_{tot}$	$\overline{\sigma}_{rad}$	KARMEN Exp.	LAMPF Exp.
$^{12}_{6}\mathrm{C}(\nu_e, e^-)^{12}_{7}\mathrm{N}$	0.14	-	0.15 ± 0.03 [53]	0.14 ± 0.03 [29]
$^{37}\mathrm{Cl}$ $(\nu_e, e^-)^{37}\mathrm{Ar}$	1.8	1.4		
$^{40}\mathrm{Ar}$ $(\nu_e, e^-)^{40}\mathrm{K}$	1.9	1.3		
$^{71}\mathrm{Ga}$ $(\nu_e, e^-)^{71}\mathrm{Ge}$	4.0	2.7		
$^{81}\mathrm{Br}$ $(\nu_e, e^-)^{81}\mathrm{Kr}$	4.5	3.2		
$^{98}\mathrm{Mo}$ $(\nu_e, e^-)^{98}\mathrm{Tc}$	5.3	2.7		
$^{115}\mathrm{In}$ $(\nu_e, e^-)^{115}\mathrm{Sn}$	7.2	4.7		
$^{127}\mathrm{I}$ $(\nu_e, e^-)^{127}\mathrm{Xe}$	7.3	4.3		6.2 ± 2.5 [30]
$^{205}\mathrm{Tl}$ $(\nu_e, e^-)^{205}\mathrm{Pb}$	14.0	6.3		

renormalization of g_A by means of the *ph* and Δh RPA excitation which leads to quenched values of g_A. Hence, the results of [57] are about a factor of two smaller than those given by the LDA.

In the experiment at Los Alamos with muon neutrinos [30], they obtain the cross section $\overline{\sigma} = [11.3 \pm 0.7\ (\text{stat.}) \pm 1.8\ (\text{syst.})] \times 10^{-40}\,\text{cm}^2$ averaged over the ν_μ flux in the range of $123.7 < E_\nu < 280$ MeV for the $^{12}\text{C}\ (\nu_\mu, \mu^-)X$ reaction. Averaging over the same distribution the LDA method gives $\overline{\sigma} = 19 \times 10^{-40}\,\text{cm}^2$. The theoretical calculation of the CRPA [42] provides the value $\overline{\sigma} = 20 \times 10^{-40}\,\text{cm}^2$. It is interesting that the results of the LDA and the continuum RPA agree very well in the point where this discrepancy exists.

3.3 Terrestrial Detection of Solar Neutrinos

The basic neutrino–nucleus reactions, which are important in solar-neutrino (antineutrino) detection experiments are shown in Table 1 of [16]. The main characteristics of these detectors [3–5] can be summarized as follows. The majority of the nuclides ^{37}Cl, ^{71}Ga, ^{81}Br, ^{98}Mo, ^{127}I and ^{205}Tl is appropriate for experiments of radiochemical type, while ^{40}Ar and ^{115}In can be employed in direct-counting experiments. The ^{37}Cl detector experiment, operating for a long time at Homestake [1,5], is sensitive only to neutrino energies above $E_{\text{thres}} = 0.814$ MeV. The two ^{71}Ga solar-neutrino detectors, at Gran Sasso and Baksan [4], have a threshold of only 0.233 MeV and are used for measuring the flux of *p p* neutrinos. ^{81}Br, proposed as a solar-neutrino detector [5], has a threshold energy $E_{\text{thres}} = 0.471$ MeV. ^{127}I can be used as a promising solar-neutrino candidate to cover the region between ^{71}Ga and the water detector Čerenkov chamber. Measurements of ^{127}I can be used to calibrate the cross sections of the ^{8}B and ^{7}Be neutrinos, since ^{127}I is sensitive to both of them. At present an experiment with ^{127}I is under way at LAMPF [29,30].

The detectors ^{205}Tl and ^{98}Mo could be used in geochemical experiments. ^{98}Mo has already been tested at LAMPF, since the ^{98}Mo detector could be used for measuring the flux of ^{8}B neutrinos averaged over the last several million years. The threshold for the neutrino reaction $^{98}\text{Mo}(\nu_e, e^-)^{98}\text{Tc}$ is $E_{\text{thres}} = 1.68$ MeV but, because the ground state and the first excited state of ^{98}Tc are forbidden, effectively $E_{\text{thres}} > 1.74$ MeV. The use of ^{205}Tl as a solar-neutrino detector would have the smallest threshold energy, $E_{\text{thres}} = 0.062$, which reflects its sensitivity to *p p* neutrinos. The proposal for a geochemical experiment on ^{205}Tl [3] suggests measuring the concentration of the ^{205}Pb isotope produced by solar neutrinos in natural ores.

From the promising direct-counting detectors, the liquid ^{40}Ar detector at Gran Sasso (ICARUS experiment) is optimized to observe solar neutrinos and it has

a threshold energy $E_{\text{thres}} = 5.885$ MeV. The ^{115}In isotope has been proposed [2] as a liquid scintillator solar-neutrino detector, because it has a very low threshold $E_{\text{thres}} = 0.119$ MeV. The produced ^{115}Sn is in the second excited $((7/2)^+)$ state.

By using the LDA method discussed before, we calculated total cross sections for the above nuclei for inclusive and semi-inclusive (anti)neutrino–nucleus processes. The results for the total cross sections as a function of the neutrino energy (in the region $50 \leq E_\nu \leq 500$ MeV) are shown in Fig. 6.

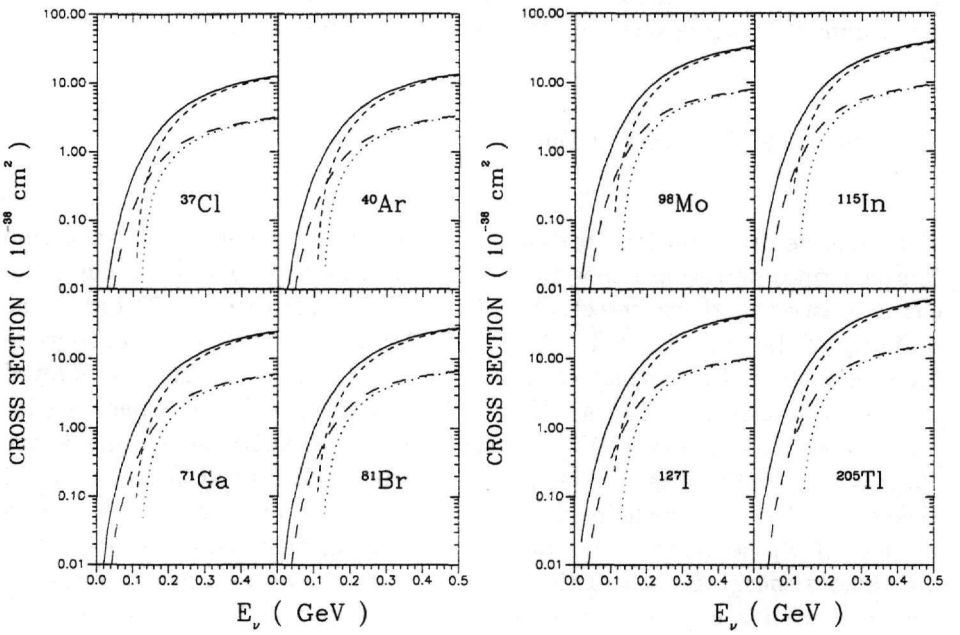

Fig. 6. Total cross sections of neutrino-nucleus induced reactions for certain promising neutrino detection nuclear targets. The curves plotted refer to the reactions: $(A,Z)(\nu_e, e^-)(A, Z+1)$ (*solid line*), $(A,Z)(\nu_\mu, \mu^-)(A, Z+1)$ (*long-dashed line*), $(A,Z)(\overline{\nu}_e, e^+)(A, Z-1)$ (*short-dashed line*) and $(A,Z)(\overline{\nu}_\mu, \mu^+)(A, Z-1)$ (*dotted line*)

As can be seen, the common characteristics of the total cross sections is that they rise appreciably at low energies but the growth becomes moderate at higher energies. In the same nucleus there are differences between the neutrino and antineutrino reactions but for each target the electron neutrino cross sections in the region $300 \leq E_\nu \leq 500$ MeV are about equal to the corresponding muon neutrino cross sections, and the electron antineutrino cross sections are about equal to those of the muon antineutrino.

By using the results of Fig. 5 and the folding method described in Sect. 2.3 we obtained the flux-averaged cross sections shown in Table 3 (see Sect. 3.2 for the discussion).

As has been discussed in Sect. 2.1, neutral-current neutrino-scattering processes could be affected by a possible sea of $s\bar{s}$ quarks in the nucleon. Since the magnitude of the strangeness content of the nucleon is unknown, recently it was proposed to extract the strangeness form factors of (10) from a measurement of neutrino-scattering cross sections [21]. A quantity especially sensitive to the strange axial form factor G_A^s is given by the ratio R_y of proton-to-neutron neutrino-induced quasi-elastic yield on ^{12}C. This can be illustrated by a simple rule of thumb for R_y by neglecting final-state interactions and assuming that the axial-vector current gives the dominant contribution to the cross section; the ratio of the proton-to-neutron neutrino-induced yield is given by (for $N = Z$ nuclei, and the axial form factor set to $G_A^3 = 1.25$)

$$R_y := \frac{(\nu, \nu' p)}{(\nu, \nu' n)} = \frac{(G_A^p)^2}{(G_A^n)^2} = \frac{\left(-\frac{1}{2}G_A^3 + \frac{1}{2}G_A^s\right)^2}{\left(+\frac{1}{2}G_A^3 + \frac{1}{2}G_A^s\right)^2} \approx 1 - \frac{16}{5}G_A^s + \ldots . \qquad (27)$$

This approximately linear dependence of R_y on the strange-quark axial form factor G_A^s is confirmed within a more sophisticated continuum RPA calculation and has been proposed as a sensitive way to measure G_A^s at LAMPF [21]. In Fig. 7 we show the results of this calculation obtained with the $\overline{\nu}_\mu$ (upper part) and ν_μ (lower part) fluxes available at LAMPF.

4 Implications to Astrophysical and Atmospheric Neutrinos

4.1 Supernova-Neutrino Studies with Water Čerenkov Detectors

The studies of the decay channels of ^{16}O levels which are excited by inelastic neutral-current scattering of supernova neutrinos, ν_x ($x = \mu, \tau$), have been proved to be of significant importance. Based on neutrino scattering off ^{16}O, the identification of supernova ν_μ and ν_τ neutrinos in water Čerenkov detectors could be achieved. This is mainly based on two facts: (i) The new super-Kamiokande (SK) detector has a lower threshold of $E_{\rm th} = 5$ MeV [58]. (ii) The daughter nuclei ^{15}N and ^{15}O, that are left over after neutrino-induced knockout of a nucleon on ^{16}O, both have first excited states with energies larger than 5 MeV ($E^* = 5.27$ MeV in ^{15}N and $E^* = 5.18$ MeV in ^{15}O [59]).

The detection scheme is shown in Fig. 8 where high energetic ν_μ and ν_τ neutrinos from a supernova predominantly excite 1^- and 2^- states in the giant-dipole resonance region in ^{16}O. As these resonances lie above the particle thresholds,

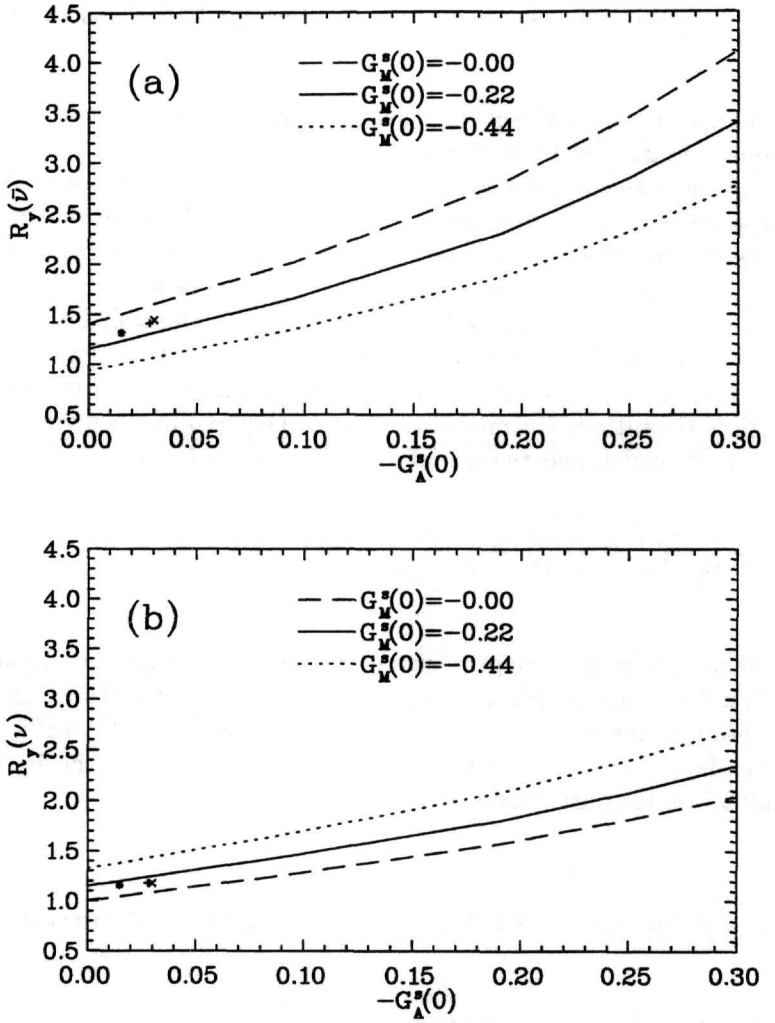

Fig. 7. Ratio of integrated proton-to-neutron yield for quasi–elastic antineutrino- (upper part) and neutrino-induced (lower part) reactions on ^{12}C as a function of $-G_A^s(0)$ for different values of $G_M^s(0)$ within the theoretically estimated regime [44,35]. The symbols indicate the predictions of a $SU(3)$ Skyrme model of the nucleon with vector mesons [45]. Their location on the horizontal axis reflects the associated prediction for $G_A^s(0)$

they dominantly decay via emission of a proton or neutron, etc.

The calculations with CRPA have shown that the 1^- and 2^- giant resonances dominantly excited by $^{16}\mathrm{O}(\nu_x, \nu_x')$ reactions mainly decay by proton and neutron emission and a significant fraction of these decays, $\approx$24% for ^{15}N and $\approx$6% for ^{15}O, do not end in the ground state of the daughter nucleus, but go to excited states, which decay by photon emission.

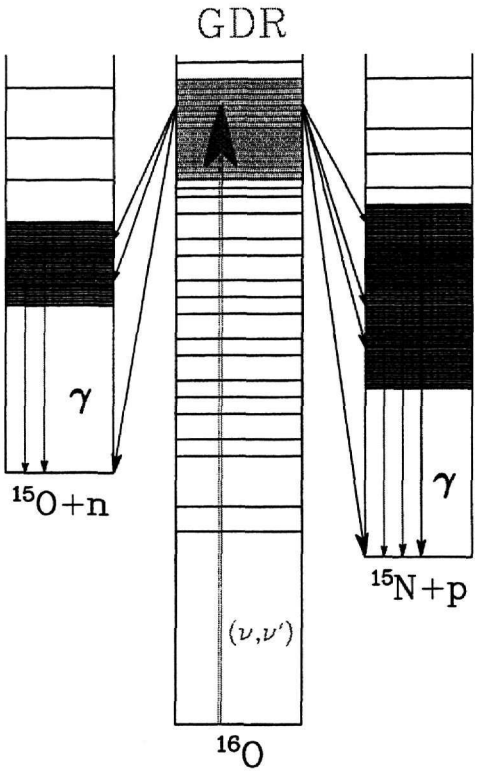

Fig. 8. Schematic illustration of the detection scheme for supernova ν_μ- and ν_τ-neutrinos in water Čerenkov detectors

One can also show that in the energy window $E = 5 - 10$ MeV this yield of photons from $(\nu, \nu' p\gamma)$ and $(\nu, \nu' n\gamma)$ reactions on ^{16}O is noticeably larger than the positron or electron background expected from other neutrino reactions in water. Therefore it constitutes a unique signal for supernova ν_μ and ν_τ neutrinos in water Čerenkov detectors.

4.2 Astrophysical Neutrino–Nucleus Interactions

Neutrino-induced reactions on nuclei play an important rôle in at least two acts of a Type II supernova spectacle. First, by scattering on the (heavy) elements in the overlying shells of the pre-supernova star, neutrinos may cause a substantial transmutation of nuclei. The main idea is that target nuclei like ^{4}He, ^{12}C, ^{16}O etc., which form major stellar burning shells through which the neutrino burst will pass, can be excited to particle-unbound states. Then, the excited levels will dominantly decay *via* emission of a proton, neutron or alpha particle (see reaction (2.4)), thus contributing to nucleosynthesis.

To estimate the effects of these processes on the natural abundances of the

elements, theoretical predictions for inelastic neutral-current neutrino scattering reactions like reaction (2.4) and for inelastic charged-current scattering reactions (or neutrino capture) represented by the scheme

$$\left.\begin{matrix} {}_{Z}A_{N}(\nu_e, e^-)_{Z+1}A^*_{N-1} \\ {}_{Z}A_{N}(\overline{\nu}_e, e^+)_{Z-1}A^*_{N+1} \end{matrix}\right\} \longrightarrow \begin{cases} \cdots + p \\ \cdots + n \\ \cdots + \alpha \end{cases} \tag{28}$$

are needed. The released p, n and α particles during these processes will further react with nuclei.

Since some of the very rare isotopes are neighbors of abundant α-shell nuclei, they could, despite the fact that neutrino-induced cross sections are so tiny, be produced in a significant amount by these processes, which have been called 'ν nucleosynthesis' [60]. In a first investigation Woosley *et al.* [60] found that the nuclei ^{7}Li, ^{11}B, ^{19}F, ^{138}La and ^{180}Ta almost entirely owe their abundance in nature to ν nucleosynthesis.

The conception is that, as the nuclei on the r-process path are weakly bound and their neutron-emission thresholds are low, their cross sections for neutrino-induced knockout of a neutron will be relatively high, and the scattering of one neutrino can lead to the emission of several neutrons. Hence theoretical predictions for the nuclear processes

$$ {}_{Z}A_{N}(\nu, \nu' j \cdot n)_{Z}X_{N-j} \, , \tag{29}$$

and

$$ {}_{Z}A_{N}(\nu_e, e^- j \cdot n)_{Z+1}Y_{N-1-j} \, , \tag{30}$$

for $j = 1, 2, 3, \ldots$ are required.

4.3 Atmospheric-Neutrino Processes

It is well known that the Earth is immersed in a flux of high-energy cosmic rays consisting mostly of protons and α particles. The upper atmosphere acts as a beam dump where these particles slow down and quickly lose their energy by creating mainly pions (and a few kaons) *via* the decays

$$\pi^{\pm} \rightarrow \mu^{\pm} + \nu_{\mu} \, (\overline{\nu}_{\mu}) \, , \tag{31}$$

$$\mu^{\pm} \rightarrow e^{\pm} + \nu_e\,(\overline{\nu}_e) + \overline{\nu}_\mu + (\nu_\mu)\,. \tag{32}$$

As we have discussed in the Introduction, the neutrino–nucleus reactions are very useful for the detection of atmospheric neutrinos and the study of atmospheric-neutrino processes. In atmospheric-neutrino experiments the nuclear structure effects are very helpful to improve the present detector simulations and choose the most appropriate target. Today there exist extensive measurements of atmospheric neutrinos. One of the recent open problems connected to atmospheric neutrinos is the so-called 'atmospheric-neutrino anomaly' described as follows.

From the decays (31) and (32) one expects the neutrino flavor ratio

$$r = \frac{\nu_\mu + \overline{\nu}_\mu}{\nu_e + \overline{\nu}_e}$$

to be about equal to 2. However, experimental measurements done up to now found that this ratio is instead equal to 1. These results have been verified from the charged-current neutrino–nucleus reactions of the type (ν_μ, μ) and (ν_e, e) in the IMB, Kamiokande and super-Kamiokande laboratories. The above discrepancy could mean that either there is a depletion of muon-type neutrinos or an enhancement of electron-type neutrinos.

In the theoretical calculations done up to now, although individual ν_e and ν_μ neutrino fluxes differ, their ratio seems to be largely model-independent, which means that the theoretical results are in clear contradiction with the data.

Up to the present there have been developed many theoretical explanations for this anomaly. One of them (see [31]) assumes the existence of a neutrino oscillation of the muon neutrinos to some other neutrino species. As a result of this oscillation the ν_μ flux appears to be reduced. Some other authors claim that this discrepancy can be ascribed to the uncertainties inherently connected to the nuclear physics and the detector used for the measured flux ratio. One of the major difficulties in such experiments is the experimental separation of the electron-type and muon-type events. In the water detectors (super-Kamiokande etc.), for example, the incoming neutrino generates an outgoing lepton *via* charged-current weak interaction with an ^{16}O nucleus. The produced lepton is detected through its Čerenkov radiation. Electrons are distinguished from the muons by the characteristics of their tracks (the track of the e^- is showering whereas the track of the μ^- is non-showering).

According to the recent super-Kamiokande atmospheric-neutrino data, the dependence of the ratio L/E_ν (where L is the traveling distance of a neutrino in vacuum and E_ν the neutrino energy) for ν_μ neutrinos can be well interpreted

by ν_μ oscillation into ν_τ. A crucial point one should mention is the fact that the atmospheric-neutrino anomaly suggests that the neutrino mixing angles could be large. Hence the interpretation one can give is intimately connected to the assumed mixing angle between ν_e and other neutrino flavors. These days, in addition to the above analysis, several other interpretations have been proposed like neutrino decay (for an extensive discussion see [31]).

5 Conclusions and Outlook

In this review we have examined the important rôle which is played by neutrinos in nuclear physics, astrophysics, high-energy physics, etc. Neutrino–nucleus reaction calculations provide theoretical studies for a number of experiments in standard 'ν' physics, in which nuclei serve as laboratories. In that case calculated results are needed for comparison with the cross sections directly measured and for predictions in order to correct for neutrino-induced background reactions. In the present work we have focused on two accurate nuclear methods used for the investigation of the neutrino–nucleus interactions: the continuum RPA that allows a straightforward evaluation in any nucleus and the local density approximation using a modified Lindhard function which makes an integration over the continuum of the excited states of a local Fermi sea. The (continuum) RPA model has the advantage that it is applicable to a wide range of weak and electromagnetic processes in nuclei (electron scattering, β decay, neutrino-scattering reactions induced by charged and neutral currents etc.). As nuclei are generally very complicated objects, nuclear models can easily fail and therefore should be tested thoroughly.

From the comparison of the theoretical results of the methods CRPA and LDA with the existing data on inclusive $^{12}\mathrm{C}(\nu_e, e^-)X$, exclusive $^{12}\mathrm{C}(\nu_e, e^-)$... and radiochemical (semi-inclusive) $^{127}\mathrm{I}(\nu_e, e^-)X$ cross sections, measured mainly at LAMPF and KARMEN, we concluded that the agreement is good. However, there is still a discrepancy on the cross section data of the reaction $^{12}\mathrm{C}(\nu_\mu, \mu^-)X$ which needs to be clarified both theoretically and experimentally. The confidence of the above methods enabled us to make predictions for astrophysical applications.

On the one hand, since the phenomenologically successful standard model is considered as a low-energy approximation, most of the physicists think that there is new physics beyond the standard model. Many experiments are performed these days which involve neutrinos to check which of the suggested extensions of the standard model is the correct theory.

Finally, the neutrino has been shown to be a very fine probe of the nucleus and the nucleons within it, and we also hope that in this respect neutrinos

at the European spallation source NESS [61] will open a new era of neutrino physics.

Acknowledgments

The authors would like to thank the Swiss National Science Foundation for partial support of this work.

References

[1] R. Davis, Jr., D.S. Harmer and K.C. Hoffman, Phys. Rev. Lett. **20**, 1205 (1968); G.S. Hurst *et al.*, Phys. Rev. Lett. **53**, 1116 (1984); R. Davis, Prog. Part. Nucl. Phys. **32**, 13 (1994).

[2] R.S. Raghavan, Phys. Rev. Lett. **37**, 259 (1976); J.N. Bahcall *et al.*, Phys. Rev. Lett. **40**, 1351 (1978); W.C. Haxton, Phys. Rev. Lett. **60**, 768 (1988).

[3] J.N. Bahcall and R.K. Ulrich, Rev. Mod. Phys. **60**, 297 (1988); K. Kubodera and S. Nozawa, Int. J. Mod. Phys. E **3**, 101 (1994).

[4] A.I. Abazov *et al.*, Phys. Rev. Lett. **67**, 3332 (1991); P. Anselmann *et al.*, Phys. Lett. B **285**, 376 (1992); K.S. Hirata *et al.*, Phys. Rev. Lett. **63**, 16 (1989).

[5] J. Rapaport *et al.*, Phys. Rev. Lett. **47**, 1518 (1981); *ibid.* **54**, 2325 (1985); D. Krofcheck *et al.*, Phys. Rev. Lett. **55**, 1051 (1985); Phys. Lett. B **189**, 299 (1987); Yu.S. Lutostansky and N.B. Skul'gina, Phys. Rev. Lett. **67**, 430 (1991).

[6] B. Bodmann *et al.*, Phys. Lett. B **280**, 198 (1992); B. Zeitnitz, Prog. Part. Nucl. Phys. **32**, 351 (1994).

[7] G. Drexlin *et al.*, KARMEN Collab., in Proceedings of the *Neutrino Workshop*, Heidelberg 1987, edited by B. Povh and H.V. Klapdor-Kleigrothaus, Springer-Verlag, 1998 p. 147.

[8] D. Bodmann *et al.*, KARMEN Collab., Phys. Lett. B **267**, 321 (1991).

[9] B.E. Bodmann *et al.*, KARMEN Collab., Phys. Lett. B **332**, 251 (1994).

[10] W. Fetscher, Phys. Rev. Lett. **71**, 2511 (1993).

[11] G. Drexlin *et al.*, KARMEN Collab., Prog. Part. Nucl. Phys. **32**, 375 (1994).

[12] T.W. Donnelly and J.D. Walecka, Phys. Lett. B **41**, 275 (1972); T.W. Donnelly, Phys. Lett. B **43**, 93 (1973); J.B. Langworthy, B.A. Lamers and H. Uberall, Nucl. Phys. A **280**, 351 (1977); E.V. Bugaev *et al.*, Nucl. Phys. A **324**, 350 (1979).

[13] B. Goulard and H. Primakoff, Phys. Rev. **135B**, 1139 (1964);
J.S. Bell and C.H. Llewellyn-Smith, Nucl. Phys. B **28**, 317 (1971).

[14] T.K. Gaisser and J.S. O'Connell, Phys. Rev. D **34**, 822 (1986); T. Kuramoto, M. Fukugita, Y. Kohyama and K. Kubodera, Nucl. Phys. A **512**, 711 (1990).

[15] S.K. Singh and E. Oset, Phys. Rev. C **48**, 1246 (1993); Nucl. Phys. A **542**, 587 (1992).

[16] T.S. Kosmas and E. Oset, Phys. Rev. C **53**, 1409 (1996).

[17] M. Buballa, S. Drożdż, S. Krewald and J. Speth, Ann. Phys. **208**, 346 (1991).

[18] E. Kolbe, K. Langanke, S. Krewald and F.K. Thielemann, Nucl. Phys. A **540**, 599 (1992).

[19] K. Nakayama, S. Drożdż, S. Krewald and J. Speth, Nucl. Phys. A **470**, 573 (1987).

[20] R. Machleidt, K. Holinde and Ch. Elster, Phys. Rep. **149**, 1 (1987).

[21] G.T. Garvey, S. Krewald, E. Kolbe and K. Langanke, Phys. Lett. B **289**, 249 (1992); G.T. Garvey, E. Kolbe, K. Langanke and S. Krewald, Phys. Rev. C **48**, 1919 (1993).

[22] H. Überall, Phys. Rev. **126**, 876 (1962); Phys. Rev. B **137**, 502 (1965).

[23] F.J. Kelly and H. Überall, Phys. Rev. **158**, 987 (1967); Phys. Rev. C **5**, 1432 (1972).

[24] T.W. Donnelly and R.D. Peccei, Phys. Rep. **50**, 1 (1979).

[25] J.D. Walecka, in *Muon Physics*, edited by V.W. Hughes and C.S. Wu, Academic Press, New York, 1975, p. 113.

[26] J.S. O'Connell, T.W. Donnelly and J.D. Walecka, Phys. Rev. C **6**, 719 (1972).

[27] T.W. Donnelly and J.D. Walecka, Phys. Lett. B **41**, 275 (1972); T.W. Donnelly, *ibid.* **43**, 93 (1973); T.W. Donnelly *et al.*, *ibid.* **49**, 8 (1974); T.W. Donnelly and R.D. Peccei, *ibid.* **65**, 196 (1976).

[28] K. Kubodera and S. Nozawa, Int. Journ. Mod. Phys. **3**, 101 (1994);
S. Nozawa, Y. Kohyama and K. Kubodera, Progr. Theor. Phys. **70**, 892 (1983).

[29] D.A. Krakauer *et al.*, Phys. Rev. C **45**, 2450 (1992).

[30] H.J. Kim, LSND Collab., data presented at *PANIC 1996.*

[31] A. Faessler, the recent super-Kamiokande data, Present Volume, p. 1.

[32] C. Athanassopoulos *et al.*, LSND Collab., Phys. Rev. C **55**, 2078 (1997); *ibid.* **56**, 2806 (1997).

[33] J. Ashman *et al.*, EMC Collab., Nucl. Phys. B **328**, 1 (1989).

[34] L.A. Ahrens et al., Phys. Rev. D **35**, 785 (1987).

[35] R.L. Jaffe and A. Manohar, Nucl. Phys. B **337**, 509 (1990).

[36] M.J. Musolf, T.W. Donnelly, J. Dubach, S.J. Pollock, S. Kowalski and E.J. Beise, Phys. Rep. **239**, 1 (1994).

[37] E.J. Beise and R.D. McKeown, Comm. Nucl. Part. Phys. **20**, 105 (1991).

[38] S.L. Mintz and M. Pourkaviani, Phys. Rev. C **40**, 2458 (1989); J. Phys. G: Nucl. Part. Phys. **16**, 569 (1990); *ibid.* **17**, 1139 (1991).

[39] S. Krewald, K. Nakayama and J. Speth, Phys. Rep. **161**, 103 (1988).

[40] J.J. Cowan, F.-K. Thielemann and J.W. Truran, Phys. Rep. **208**, 267 (1991).

[41] E. Kolbe, Ph.D. Thesis, Universität Münster (1992).

[42] E. Kolbe, K. Langanke and S. Krewald, Phys. Rev. C **51**, 1122 (1995).

[43] S.L. Mintz and M. Pourkaviani, Nucl. Phys. A **584**, 665 (1995).

[44] R.L. Jaffe, Phys. Lett. B **229**, 275 (1989).

[45] E. Kolbe, S. Krewald and H. Weigel, Z. Phys. A **358**, 445 (1997).

[46] H.C. Chiang, E. Oset and P. Fernandez de Cordoba, Nucl. Phys. A **510**, 591 (1990); H.C. Chiang, E. Oset, R.C. Carrasco, J. Nieves and J. Navarro, Nucl. Phys. A **510**, 573 (1990).

[47] E. Oset, P. Fernandez de Cordoba, L.L. Salcedo and R. Brockmann, Phys. Reports **188**, 79 (1990).

[48] E. Oset, D. Strottman, H. Toki and J. Navarro, Phys. Rev. C **48**, 2395 (1993).

[49] H. Überall, Nuovo Cim. **23**, 219 (1962).

[50] R.L. Burman, private communication; R.L. Burman, M.E. Potter and E.S. Smith, Nucl. Instrum. Meth. Phys. Res. Sect. A **291**, 612 (1990).

[51] R.C. Allen, H.H. Chen, P.J. Doe, R. Hausamann and W.P. Lee, Phys. Rev. Lett. **64**, 1871 (1990).

[52] LAMFP Research Proposal LA-UR-89-3764 (1989), Spokesman: W.C. Louis.

[53] B. Armbruster *et al.*, KARMEN Collab., Phys. Lett. B **423**, 15 (1998).

[54] T. Suzuki *et al.*, Phys. Rev. C **35**, 2212 (1987).

[55] J. Kleinfeller *et al.*, in *Neutrino '96,* edited by K. Enquist, H. Huitu and J. Maalampi, World Scientific, Singapore, (1997).

[56] R. Imlay, Nucl. Phys. A **629**, 531c (1998) and private communication (1998).

[57] J. Engel, S. Pittel and P. Vogel, Phys. Rev. C **50**, 1702 (1994).

[58] Y. Totsuka, Rep. Progr. Phys. **55**, 377 (1992).

[59] F. Ajzenberg-Selove, Nucl. Phys. A **523**, 1 (1991).

[60] S.E. Woosley, D.H. Hartmann, R.D. Hoffman and W.C. Haxton, Astrophys. J. **356**, 272 (1990).

[61] G. Drexlin, J. Kleinfeller, B. Zeitnitz and R. Maschuw, *NESS: Neutrinos at the European Spallation Source*, Internal Report (1996).